




Nuclear structure advancements with multi-nucleon transfer reactions

R. M. Pérez-Vidal^{1,2}, F. Galtarossa³, T. Mijatović⁴, S. Szilner⁴, I. Zanon², D. Brugnara², J. Pellumaj^{2,5}, M. Ciemala⁶, J. J. Valiente-Dobón², L. Corradi², E. Clément⁷, S. Leoni^{8,9}, B. Fornal⁶, M. Siciliano¹⁰, A. Gadea^{1,a} 

¹ Instituto de Física Corpuscular, CSIC - Universidad de Valencia, Valencia 46980, Spain

² Istituto Nazionale di Fisica Nucleare, Laboratori Nazionali di Legnaro, Legnaro 35020, Italy

³ Istituto Nazionale di Fisica Nucleare, Sezione di Padova, Padova 35131, Italy

⁴ Ruđer Bošković Institute, Zagreb 10000, Croatia

⁵ Dipartimento di Fisica e Scienze della Terra, Università degli Studi di Ferrara, Ferrara 44121, Italy

⁶ The Henryk Niewodniczański Institute of Nuclear Physics - PAN, Kraków 31-342, Poland

⁷ Grand Accélérateur National d'Ions Lourds, CEA/DRF-CNRS/IN2P3, 14076 Caen Cedex 5, France

⁸ Istituto Nazionale di Fisica Nucleare, Sezione di Milano, Milan 20133, Italy

⁹ Dipartimento di Fisica, Università di Milano, Milan 20133, Italy

¹⁰ Physics Division, Argonne National Laboratory, Lemont 60439, IL, USA

Received: 23 March 2023 / Accepted: 4 May 2023

© The Author(s) 2023

Communicated by Nicolas Alamanos

Abstract Multi-Nucleon Transfer (MNT) reactions have been used for decades as a reaction mechanism, in order to populate excited states in nuclei far from stability and to perform nuclear structure studies. Nevertheless, the development of set-ups involving high acceptance tracking magnetic spectrometers (mainly existing in Europe), coupled with the Advanced GAMMA Tracking Array (AGATA) opens new possibilities, especially if they are used in conjunction with high-intensity stable beams or ISOL RIBs. In this article, we will discuss the capabilities of such set-ups aiming at different goals, including complete information in high-resolution spectroscopy as well as lifetime measurements.

1 Introduction

Multi-nucleon transfer reactions are generally defined as reactions transferring one or more nucleons when using “heavy” nuclei ($Z > 2$) as projectiles and targets. The MNT reactions, in both quasi-elastic (QE) and deep-inelastic collision (DIC) regimes, were broadly used in the late 60’s and the 70’s for the production of new isotopes. Already in this period, the capability of these reactions to produce neutron-rich nuclei was discussed [1]. It was also suggested the “Charge equilibration” mechanism, a very relevant aspect in connection with the role of MNT reactions in nuclear structure studies [2]. Experimental works involving γ -ray

detection, following MNT in both aforementioned regimes, initially focused on evaluating the degree of spin polarisation/alignment in the reaction products (e.g. [3–5]). Early nuclear structure studies used MNT reactions as a production method, performing decay spectroscopy studies following mass separation (e.g. [6–8]). The advent of the set-ups with multiple Ge detectors in the early 90’s opened the possibility to perform in-beam nuclear structure studies using MNT reactions and a thick target, i.e. stopping the reaction products (e.g. Refs. [9–13]). In such experiments, the absence of the reaction product identification requires previous knowledge of γ -ray transitions in the nucleus of interest, for example from spectroscopy following β -decay, to be able to build the nuclear level scheme. A relevant landmark, in the use of MNT reactions in nuclear structure studies, arrived in the early 2000’s with the construction of large acceptance tracking magnetic spectrometers VAMOS++ [14–16] at the GANIL laboratory in France and PRISMA [17, 18] at the INFN LNL in Italy, and the early coupling of them with Ge detector arrays: EXOGAM [19] with VAMOS++, CLARA [20] with PRISMA, the AGATA Demonstrator [21] with PRISMA and implementations of AGATA with both VAMOS++ [22] and PRISMA [23]. The direct measurement of the de-exciting γ rays in coincidence with the reaction products, identified in A and Z by the spectrometers and with the information on the trajectory, is fundamental for the assignment of the structure information to the nucleus of interest and to perform Doppler correction for the emitted γ

^a e-mail: gadea@ific.uv.es (corresponding author)

rays. The coupling of the large Ge arrays with VAMOS++ and PRISMA also opened the possibility to perform lifetime measurements, using Doppler techniques, since the trajectory and velocity of the reaction products are reconstructed from the information provided by the entrance and focal plane detectors of the spectrometers, e.g. Ref. [24], with the differential Recoil Distance Doppler shift (RDDS) technique. In the following sections, the advancements and potential use of MNT reactions for nuclear structure studies will be reported, together with descriptions and examples of the experimental techniques and instrumentation developed.

2 Multi-nucleon transfer reactions with stable and radioactive beams as a mechanism to investigate the structure of moderately neutron- and proton-rich nuclei

MNT reactions between heavy ions at energies close to the Coulomb barrier are characterised by the exchange of many nucleons between the target and the projectile and represent the largest part of the total reaction cross section [25,26]. They provide the main mechanism for the energy dissipation from the relative motion to the intrinsic excitation. Typically, a population of relatively low excitation energy and relatively high spins is observed in the final reaction products [25–28].

In heavy-ion-induced transfer reactions, the exchange of the mass, charge, energy, and angular momentum between reaction partners is mediated by the single-particle (fermion) and surface vibration (boson) properties of the two colliding ions [25]. One thus expects that the same degrees of freedom will play an important role in the description of the states populated in these transfer reactions. In fact, the states populated in transfer channels show the direct population of the states of single-particle character, as well as the population of states that involve combinations of a single particle or hole with a collective boson [29–32]. In the case of the fermion-boson coupling, the transfer mechanism will not populate all components of the expected multiplet uniformly, but will always favour the more stretched configurations, as the transfer probability will have a maximum at the largest angular momentum transfer. This in turn is connected to the requirement of the smooth matching of the entrance and exit channel trajectories [33]. The same mechanism is at the origin of a strong population of the yrast and near-yrast states [34–37].

The expected population of neutron-rich nuclei is based on the results of state-of-the-art calculations developed by the theoretical group at the Niels Bohr Institute [38]. Recently, other theoretical approaches, using different mechanisms, supported this idea [39–46], though not necessarily providing the same neutron richness, emitting angles, and energies of the fragments. To understand how to approach this neutron-rich region, one has to keep in mind that transfer processes

are mainly governed by reaction dynamics and by the spectroscopic information of colliding nuclei (form factors), and by the balance of the internal and binding energy in the phase space of the colliding systems (optimum Q -value considerations) [25].

Due to the characteristic behavior of the binding energy in the nuclear chart, the process is essentially governed by the lighter partner of the reaction. In general, the use of lighter stable projectiles on heavy targets results in activating only proton-stripping and neutron-pick-up channels (the terms pick-up and stripping are conventionally referred to the lighter partner of the reaction), thus, populating moderately neutron-rich mid-mass nuclei. With neutron-rich projectiles, proton-pick-up and neutron-stripping channels also open up, leading to the population of the neutron-rich heavy fragments [47–52].

As an example, Fig. 1 shows the total experimental cross sections for ^{40}Ar (the most neutron-rich stable Ar isotope), ^{40}Ca (closed-shell nucleus), and ^{58}Ni (open-shell nucleus) induced reactions on a ^{208}Pb target, together with the corresponding theoretical prediction [50,53–55]. The measured cross sections clearly illustrate that the dominant channels are neutron pick-up and proton stripping ones. Only in the case where the most neutron-rich stable isotope is used, the proton pick-up and neutron stripping channels develop, and for the very neutron-rich (unstable) projectiles these channels become dominant [38]. This path, relevant for the population of neutron-rich heavy partner, is illustrated in Fig. 2, where the total cross sections for Pb isotopes in the $^{40}\text{Ar}+^{208}\text{Pb}$ and $^{94}\text{Rb}+^{208}\text{Pb}$ collisions are displayed [50,52,56]. Heavy fragments were identified via their characteristic electromagnetic transitions. The reactions with radioactive beams, like in the case of the $^{94}\text{Rb}+^{208}\text{Pb}$ system measured with MINIBALL [57] coupled to an annular position sensitive silicon detector, demonstrate that MNT are in fact suitable mechanisms to reach neutron-rich nuclei close to the $N = 126$.

Valuable insight into the role of the pair (neutron and/or proton) transfer in the MNT reactions was obtained by coupling the large solid angle magnetic spectrometers and γ arrays which allowed to investigate nucleon–nucleon correlations induced by the pairing interaction in more details. In this respect, AGATA (up to 2π) is fundamental to measure the distribution of the total transfer cross section over different states [58–60].

When more and more nucleons are transferred, the transition from a regime of quasi-elastic to the more damped regime of deep inelastic occurs. While the quasi-elastic reactions show the characteristics of the direct reactions (the bell shape angular distribution with a maximum close to the grazing angle), the deep-inelastic processes are characterised by a massive transfer of nucleons (toward the charge equilibration, namely the N/Z ratio of the compound nucleus) and very large energy losses [25,61–64]. In measurements where

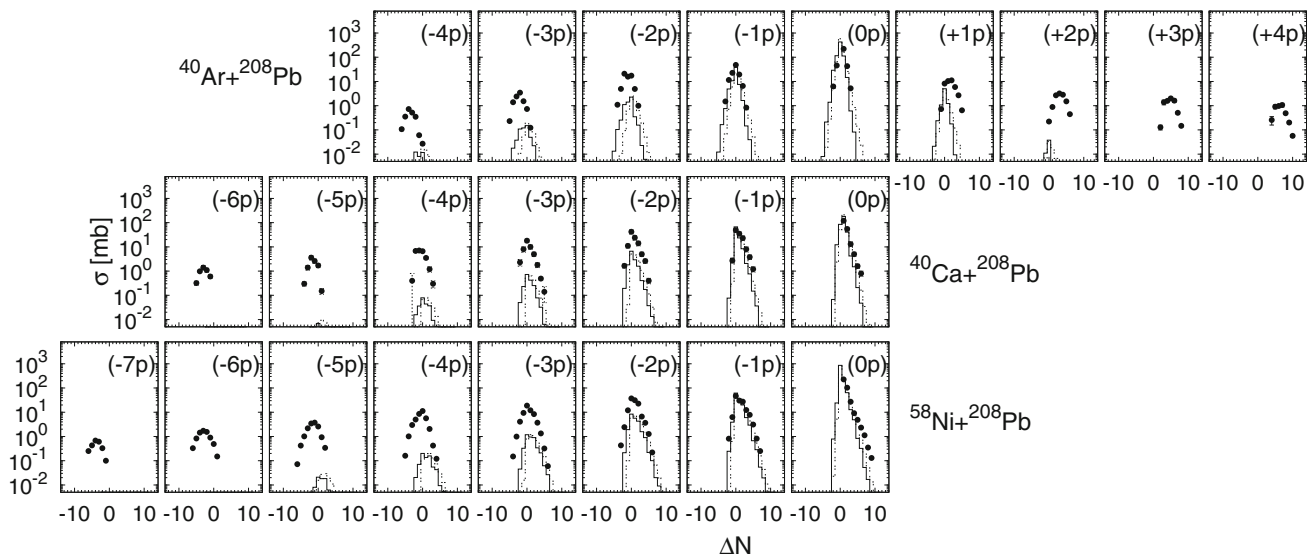


Fig. 1 Total experimental cross sections for ^{40}Ar , ^{40}Ca , and ^{58}Ni induced reactions on the ^{208}Pb target, at beam energies $E_{\text{lab}} = 6.4$, 6.2, and 6 MeV/u, respectively (points), and the GRAZING calcula-

tions with (solid line) and without (dashed line) neutron evaporation (as published in Ref. [50] with data from Refs. [50,54,55])

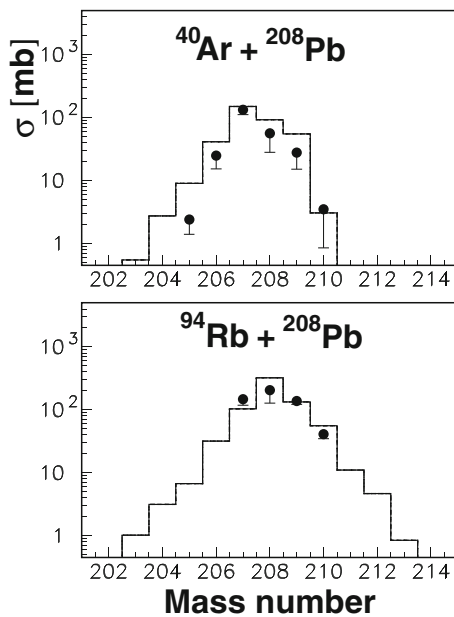


Fig. 2 Total cross section for Pb isotopes in $^{40}\text{Ar} + ^{208}\text{Pb}$ and $^{94}\text{Rb} + ^{208}\text{Pb}$ collisions. In the $^{94}\text{Rb} + ^{208}\text{Pb}$ reaction, the measured cross sections obtained with the γ -ray measurement are indicated as lower limits, while those which include the estimated values for the ground states are indicated with full points. In the case of the $^{40}\text{Ar} + ^{208}\text{Pb}$, the fragment cross sections obtained with the γ -ray measurement are indicated as lower limits, while the total cross sections (measured in PRISMA) are indicated with full points. The histograms are the GRAZING predictions. Data taken from Refs. [50,52,56]

the transfer products have been identified close to the grazing angle, the observed final nuclei do not reach the N/Z ratio of the compound nucleus, due to the dominance of a direct mechanism [25]. On the other hand, A and Z distribu-

tions closer to the charge equilibration have been observed in measurements that integrate all scattering angles, and consequently the whole range of energy losses, for example in the thick target measurements [61,65].

The transition from the quasi-elastic to deep-inelastic regimes has been the subject of very large amount of studies (see for example Ref. [62]), but the understanding of their details still faces significant experimental and theoretical challenges. In particular, it will be important to understand how the scattering angle of the quasi-elastic and deep-inelastic components develop as a function of the charge and the mass of the reaction fragments. While for the lighter systems, it is expected that the large energy losses will occur at the more forward angles connected with the smaller impact parameters, for the heavier systems where the Coulomb repulsion dominates, the quasi-elastic and deep-inelastic components scatter at an almost same angle in a quite energy loss independent way. Finally, with the very strong Coulomb field, a monotonic increase of the scattering angle for increasing kinetic energy was observed [62]. It would be important to test these findings in higher resolution measurements (see for example Refs. [50,66,67]).

In recent measurements, reactions induced by lighter ions (with $A = 10\text{--}24$) on medium-mass or heavy targets turn out to be very effective for the production and spectroscopic studies of light exotic nuclei [68–71], as well, even employing radioactive ion beams [72]. In these processes, in spite of the rather low masses of projectile-like fragments, the large energy losses have been measured. The experimental data, which are rather limited for these light fragments, are well reproduced by the model based on Langevin-type equations

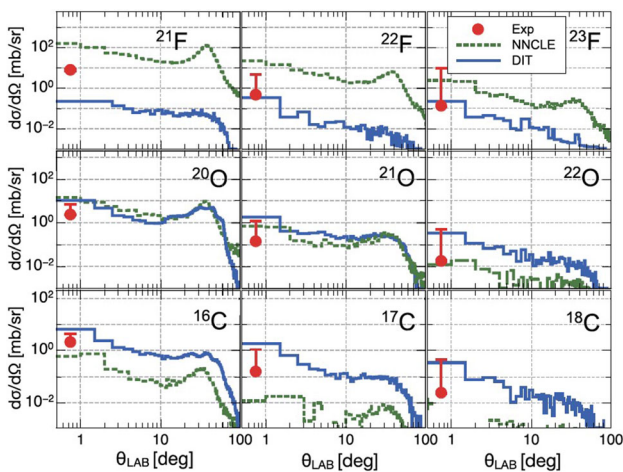


Fig. 3 Comparison between data (red symbol) and calculations with the deep inelastic models (NNCLE+NEV [76,77] and DIT+GEMINI++ [63,78]) for selected nuclei obtained from a high-intensity ^{18}O beam (at 8.5 MeV/u) on a ^{238}U target (1 mg/cm² thick). The experimental measurement, at 0°, was performed at GANIL with the LISE spectrometer [74]

of motion [73]. In addition, in the reaction of ^{18}O impinging on a ^{238}U target [74] measured using the LISE achromatic spectrometer of GANIL [75], cross sections were extracted at zero degrees. Sizable cross sections were found for the production of exotic species connected with the neutron pick-up and proton stripping channels, as illustrated in Fig. 3.

Deep-inelastic reaction product cross sections at zero degree were as well studied, though at much higher energies (Fermi energies) and in general with heavier beams, by Souliotis, Veselsky and collaborators (see e.g. in Refs. [79,80]), with the MARS [81] and MAGNEX [82,83] spectrometers. These studies aimed to define optimal projectile-target combination and beam energies for the production of exotic species, suggesting that, with the determined cross sections, these reactions could be a competitive mechanism for radioactive ion beam production.

In reactions where large energy losses are present, secondary processes, such as neutron evaporation, may significantly influence the final isotopic distributions. They generally shift the mass distributions toward lower values. Very few measurements have been performed so far with the extracted cross sections of both binary fragments [47,48,51,52,84]. Even if the results demonstrate that the most neutron-rich final isotopes are produced through collisions involving small kinetic energy losses [47,51], it is essential to establish the best experimental conditions for the largest survival probability of the neutron-rich nuclei. In spite of the unavoidable lowering of the final yield due to the onset of secondary processes, the measured rates are suitable for spectroscopic studies with the existing (and possibly upgraded) γ -ray detector arrays and fragment spectrometers

[14,15,18,19,21,27,85,86], especially in the light of the future radioactive facilities such as SPIRAL2 at GANIL and SPES at LNL [87,88].

3 High-acceptance tracking magnetic spectrometers: status and outlook

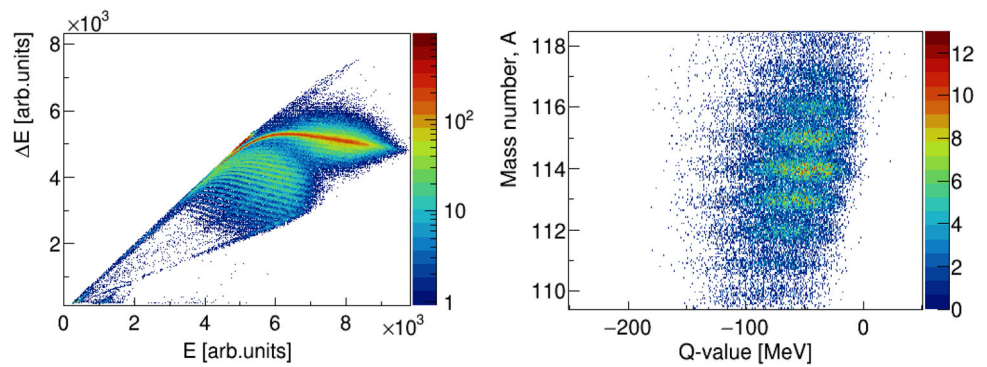
The study of nuclear structure and reaction dynamics by means of MNT reactions requires the use of large-acceptance detectors with high mass and charge resolution to unambiguously identify the different isotopes populated in the reaction. This has been achieved, in the last two decades, through the development of large solid angle (~ 100 msr) magnetic spectrometers, like PRISMA [17,18] installed at INFN-LNL, Italy, VAMOS++ [14–16] at GANIL, France and MAGNEX [82,83] at INFN-LNS, Italy.

Magnetic spectrometers select the incoming ions according to their magnetic rigidity $B\rho$, which is equal to the momentum-over-charge ratio, p/q . The mass identification is performed on an event-by-event basis by measuring the Time-of-Flight (ToF) of the ions in the spectrometer and reconstructing their trajectories in the magnetic elements. The nuclear charge is measured via the $\Delta E - E$ method in a segmented Ionisation Chamber (IC), placed at the end of the spectrometer, where the ions of interest are stopped. To ensure mass separation, while dealing with heavier and heavier ions, position information becomes crucial. The presently adopted solution for large solid angle spectrometers is the simplified magnetic element configuration and the use of the concept of trajectory reconstruction. The detector system in these spectrometers, besides nuclear charge, energy, and timing, provides the necessary position information along the ion path.

In these new-generation spectrometers, unequivocal identification has been successfully demonstrated for ions up to mass number $A \sim 130$ and atomic number $Z \sim 60$. An example using PRISMA is shown in Fig. 4. Mass identification up to $A \sim 200$ was achieved in Ref. [89], without Z determination and with a gate on a narrow portion of the focal plane, and by an indirect method, in even heavier elements, using the full identification of the light partner and the corresponding two-body kinematics [47,90].

One of the future challenges for MNT reactions and the corresponding prompt spectroscopy is to explore the unknown area of exotic nuclei with $N = 126$ as far as possible from the doubly-magic ^{208}Pb nucleus. To reach this goal the existing magnetic spectrometers, in particular, PRISMA and VAMOS++, are being upgraded to extend the ion identification to higher A and Z . The measurement of additional observables, such as ion velocity vector before and after the magnetic elements, ion tracks in the IC, improved trajectory reconstruction via software with the use of transport matrices

Fig. 4 (Left) Nuclear charge identification in PRISMA in the MNT reaction $^{118}\text{Sn}+^{206}\text{Pb}$ at 5.8 MeV/u in inverse kinematics at $\theta_{\text{lab}} = 25^\circ$. The most intense band represents the elastic and quasi-elastic components of target-like (Sn) particles. (Right) Mass vs Q value matrix for the $-2p$ transfer channel (Cd isotopes) in the same reaction at $\theta_{\text{lab}} = 35^\circ$. Both figures are taken from Ref. [67]



and the correction of optical aberrations, and the kinematic coincidence between light and heavy reaction partners are important ingredients in this context.

As an example, in order to obtain direct information on the behavior of the heavy reaction partner after the transfer process, the $^{197}\text{Au}+^{130}\text{Te}$ reaction at 1.07 GeV was studied, coupling PRISMA to a second arm consisting of an MWPPAC detector followed by an axial ionisation chamber [91]. The detection of the target-like Te fragments (TLF) in PRISMA with high resolution and of the projectile-like Au fragments (BLF) in the second arm allowed to construct a mass-mass correlation matrix and to follow the evolution of the centroid and width of the heavy partner mass distribution as a function of the number of transferred neutrons [51]. The alignment of the A/q loci, as a function of the ion position at the entrance and focal-plane detectors, via a recursive software procedure, was essential to reach a sufficient mass resolution to unambiguously identify the different transfer channels, as also shown in Refs. [48, 67].

The VAMOS++ detection system was upgraded during the last decade to reach a unique identification of heavy and slow fission fragments [15] (see also the *Advancements of γ -ray spectroscopy of isotopically identified fission fragments with AGATA and VAMOS++* in this topical issue).

Several developments were also started to achieve the identification of isotopes in the $N = 126$ region, in particular by constraining the velocity and scattering angle of the heavy partner as the projectile-like fragment is fully identified (Z, A) in VAMOS++. Typical experiments are performed with the ^{136}Xe beam and heavy targets such as W, Os, Pt, Pb, or U. The TLF identification is obtained from its measured velocities and kinematics and the full particle identification of the BLF. The two-body kinematics will result in a mass determination of the TLF before neutron evaporation and excitation energy of the system. This is achieved by a second arm detection system called CATLIFE composed of a set of two PPACs at 55 degrees with respect to the beam, measuring positions, and ToF [16]. Finally, EXOGAM [19] clover detectors are placed after the second PPAC for isomer tagging.

It is worth mentioning that such heavy-ion detection systems require a sizeable fraction of solid angle to be efficient and, nevertheless, are compatible with the early version (up to 2π) of the AGATA array [21–23]. On the contrary, coupling a 3π solid angle and beyond of AGATA with a unique identification of the heavy ions produced in these reactions requires novel approaches to be explored. Finally, such reactions are performed at very high counting rates at the target position. Due to the high resolving power and the high counting rate capabilities of AGATA, the prompt spectroscopy of the produced isotopes can be achieved.

At the other extreme of the nuclear chart, the identification of light ions ($A < 30$) in magnetic spectrometers can open possibilities for new physics, as discussed in Sect. 5.3. Here the main issue is represented by the low ionisation induced by light particles, which reflects in a lower efficiency of the tracking detectors of the spectrometer, and by the high acceptance in momentum required to accommodate most of the charge state distribution of these light ions. Moreover, when mass and element identification is not an issue, as for light systems, reaching more exotic systems will require higher beam intensity and therefore more counting rate in the magnetic spectrometer. The use of fully digital electronics and of a dedicated focal plane detection systems will improve the resolving power under these conditions.

4 Angular distribution and polarisation measurements in quasi-elastic and deep inelastic multi-nucleon transfer reactions

It is well known that nuclear reactions, populating states with angular momentum different from 0, leave the residual nucleus with a non-random alignment [92, 93]. Early experimental works on fragment angular momentum orientation following deep-inelastic scattering (at grazing angles) [3, 4, 94–96], concluded that there is alignment in the direction perpendicular to the reaction plane, i.e., in the direction $(\mathbf{k}_b \times \mathbf{k}_p)$, with \mathbf{k}_b and \mathbf{k}_p being the momenta of the beam and reaction product, respectively. Nevertheless, it is claimed

that it was difficult to predict the degree of alignment of the reaction product for several reasons, including the effect of evaporation. In these works it is pointed out that, when the reaction product direction is detected, it is necessary to resort to the particle-gamma angular correlation formalism given by Rybicki, Tamura, and Satchler [92,94], to determine the angular distribution as follows:

$$W(\theta_\gamma, \phi_\gamma) = \sum_{\substack{K, Q \\ K \text{ even}}} A_{K, Q} B_K Y_{K, Q}(\theta_\gamma, \phi_\gamma)$$

where $Y_{K, Q}$ are spherical harmonics, B_K the attenuation coefficient due to the detector finite resolution and $A_{K, Q}$ the angular distribution coefficients [92–94]. It is relevant to notice that the terms that will be contributing to the angular distribution depend on the choice of the coordinate system [92,93].

In order to understand the capabilities of measurements involving angular information, it is interesting to explore results obtained in experiments with large Ge-detector arrays performing angular distribution and linear polarisation measurements of γ rays emitted following MNT and DIC. In general, angular distribution results have been used for the determination of the transition multipolarities and linear polarisation measurements (together with the angular distribution information) allow one to determine the character of the transition. In this section we will mainly discuss examples performed with previous arrays to AGATA. The first one work was published by Bucurescu and collaborators [97] and reports on two experiments performed with the CLARA-PRISMA set-up [20] and GASP [98]. The latter, using a thick target, does not detect the trajectory of the reaction products. Such measurements, integrating all possible reaction angles, allow to recover the cylindrical symmetry necessary for the conventional angular distribution analysis [92,99]. The authors have determined that an alignment of about $\sigma/J \approx 0.3$ (where σ is the width of the angular momentum (J) Gaussian distribution, as in Ref. [100]) is achieved for the Rb and Y isotopes populated with transfers of up to 10 nucleons and multipolarities have been determined for the corresponding transitions using conventional techniques of angular distribution ratios with the available angles in GASP.

The second example was reported in a publication by Montanari, Leoni, and collaborators [101] and Sahin and collaborators [102], investigating the structure on neutron-rich nuclei in the vicinity of ^{48}Ca and ^{82}Se , respectively, with the nuclei of interest populated in MNT reaction. The experimental set-up was the already mentioned CLARA-PRISMA [27] and, therefore, the γ -ray data are measured in coincidence with the magnetic spectrometer PRISMA, positioned at the grazing angle. In reference [101], following the transfer of few nucleons (usually up to two), the authors find alignments of the order of $\sigma/J \approx 0.4$. With a determined trajectory of the

reaction product, it was possible to do angular distributions in both the polar θ and azimuth ϕ angles as well as to perform linear polarisation measurements using the capability of the Clover detectors of CLARA (see for example figures 6, 7 and 8 in reference [101]). Regarding the angular distributions on θ , Ge arrays with large solid angle coverage as CLARA, or AGATA in the configuration with sufficient solid angle coverage, it is possible to recover the cylindrical symmetry by integrating the detected γ rays over the azimuthal angle, taking the z-axis along the momentum direction of the reaction product being detected by the spectrometer. Again this technique allows angular distribution and angular distribution ratios to be performed in the conventional manner quoted before. Similarly, in reference [102], alignments of the order of $\sigma/J \approx 0.6$ have been determined for the Se isotopes and, taking advantage of the symmetry of CLARA on the azimuthal angle, employing angular distribution ratios (ADO Ratios), multipolarities were determined for transitions in the N=50 ^{83}As , ^{82}Ge , and ^{81}Ga nuclei (see figures 3 and 5 in reference [102]). Moreover, as mentioned, using spectrometers as PRISMA or VAMOS++ it is possible to have a well-defined direction for the ejectile emitting the γ rays, therefore, it is possible to resort as well to the angular distributions in the azimuthal angle ϕ . Figure 5, adapted from Fig. 6 of reference [101], displays the calculated angular distribution for a quadrupole stretched transition together with the measured one using the detectors with $\theta \approx 90^\circ$ of the CLARA array.

Regarding the AGATA array, the early configurations implemented with PRISMA and VAMOS++ were covering solid angles below 1π sr at nominal distances, therefore very limited experimental results are available [103]. The main goal of this section was to conclude that both angular distribution and linear polarisation measurements for the emitted γ rays in MNT reactions can be measured, recovering the cylindrical symmetry or taking into account the azimuthal angle dependency. The performance of AGATA in both angular distribution and linear polarisation measurements is discussed in other contributions to this issue [104].

5 Lifetime measurement techniques for MNT experiments

The capability to produce difficult-to-reach nuclei and how the states in these nuclei are populated (see Sect. 2) has triggered an increasing interest to perform lifetime measurements using MNT reactions. Being directly related to reduced transition probabilities, lifetimes can provide meaningful information on the structure of the nucleus and in particular on the nature of its states. With the increase in angular coverage of the γ -ray detector arrays, it is nowadays possible to have sufficient sensitivity to perform precise lifetime mea-

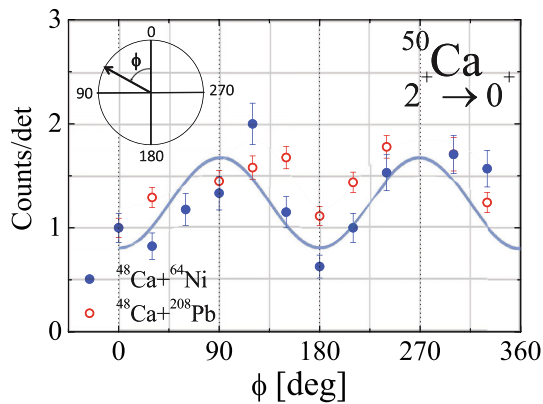


Fig. 5 Experimental vs calculated angular distribution as a function of the azimuthal angle ϕ and with $\theta \approx 90^\circ$ for an E2 transition $2^+ \rightarrow 0^+$ in ^{50}Ca , adapted from Ref. [101]. For $\theta \approx 90^\circ$ the odd Q terms of the general angular distribution equation vanish and the expression takes the form of $W(\theta_\gamma = 90^\circ, \phi_\gamma) = 1 - \frac{1}{2}A_{2,0} + \sqrt{\frac{9}{6}}A_{2,2}\cos(2\phi_\gamma) + \dots$ (see Refs. [92,93]). The blue line in the figure corresponds to the calculated value $W(\theta_\gamma = 90^\circ, \phi_\gamma)$ normalised to the relative values obtained in the experiment. The response of the CLARA detectors B_K has not been included in the calculation

measurements using Doppler-shift-based techniques such as the RDDS method [105] employing the plunger, for lifetimes in the range from few to hundreds of picosecond, and the Doppler Shift Attenuation Method (DSAM) [106], for lifetimes in the range of femtoseconds.

These two techniques rely on a precise Doppler correction that can be ensured by the angular resolution of the AGATA array coupled to a large acceptance magnetic spectrometer, such as VAMOS++ and PRISMA, providing an accurate kinematic reconstruction of the detected recoil. In fact, by measuring the emitting nuclei with such spectrometers, it is possible not only to identify and select the reaction product of interest but also to perform an event-by-event Doppler correction. In addition, by taking advantage of the Total Kinetic Energy Loss (TKEL) measurement, it is also possible to both reduce and control the contribution from the feeding transitions, that usually are major sources of systematic errors if not taken into consideration.

5.1 RDDS technique with differential plungers

The RDDS technique is a well-established method for the determination of lifetimes in the range of few picoseconds to hundreds of picoseconds [105]. In MNT reaction studies with set-ups including magnetic spectrometers, the standard technique using a stopper after the target is replaced by the one using a degrader (differential plunger). The degrader slows down the reaction products yielding two components in the γ -ray spectrum due to the different velocities (before and after the degrader) of the emitting nuclei, still with the energy

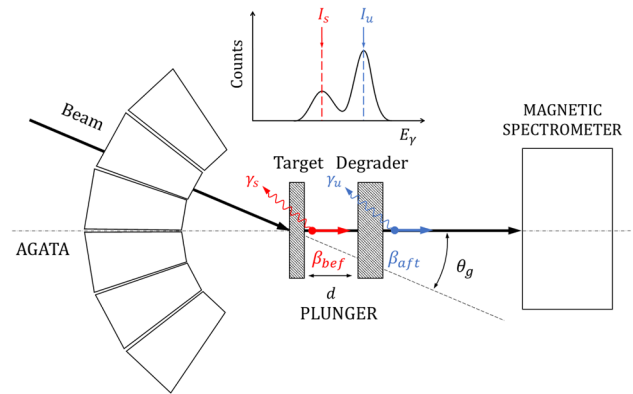


Fig. 6 Schematic view of the experimental set-up and description of the recoil distance doppler-shift method

sufficient for the identification in the magnetic spectrometers (Fig. 6).

This allows the Doppler correction of the γ rays emitted after the ions pass the degrader and its peaks appear at the correct energy (unshifted, I_u). For MNT reaction set-ups the γ rays are observed at backward angles, thus the peak of the γ ray emitted before the degrader is lowered in energy (shifted, I_s) due to the different velocity. This is schematically illustrated in Fig. 6. The ratio of the intensities of the two components I_s and I_u as a function of the target-to-degrader distance d is directly related to the lifetime of the excited state that one wants to determine. Due to the precise determination of the ion velocity vector in magnetic spectrometers, such as PRISMA and VAMOS++, and the identification of the first interaction point of the γ rays inside the AGATA array, the Doppler correction can be performed on an event-by-event basis. The superior Doppler correction provided by the AGATA position sensitivity is of paramount importance in these kinds of measurements, in which the requirements of the magnetic spectrometer for the reaction product identification, limit the difference between the velocity before and after the degrader.

The consideration of level-feeding in the analysis is crucial for the reliable determination of the lifetime. The advantage of using a spectrometer is that it permits to control partially the feeding (direct or from higher states) by means of a selection in the TKEL [107, 108]. In this way, it is possible to limit or reduce the effect of indirect feeding in the lifetime measurement of the state of interest.

As an example, lifetimes of several states in ^{90}Zr , ^{92}Mo and ^{94}Ru were measured with the RDDS technique for the first time at GANIL with AGATA and VAMOS++, in order to study the seniority conservation in the proton $g_{9/2}$ orbital for the semi magic $N = 50$ isotones [109]. In this experiment, the MNT reaction, broadly used to produce moderately neutron-rich nuclei, was unconventionally adopted to populate the states of interest below the isomers in neutron-

deficient nuclei. The $N = 50$ isotopes were produced in the collision of a ^{92}Mo beam at an energy of 717 MeV on a 0.775 mg/cm^2 ^{92}Mo target. The target was mounted on the IKP Cologne plunger [105], while a 1.9 mg/cm^2 thick ^{24}Mg foil was used to degrade the energy of the reaction products. This experiment was performed during the phase I of AGATA having 23 operational detectors. In this scenario, the condition in the detected ion TKEL could be applied to limit or reduce the contribution of the indirect feeding to the state of interest. Figure 7 illustrates the correspondence between the TKEL selection values and the population of the excited states in the ^{92}Mo nucleus. For clarity due to high statistics, the inelastic channel of the reaction is shown as an example, nevertheless, the TKEL condition was applied also to the MNT channels of the same reaction [110]. The upper panel a) shows the Doppler corrected γ -ray spectrum for ^{92}Mo and the populated states without any TKEL condition. For low values of the TKEL the population of the higher states is reduced. With this condition in panel b) the $6^+ \rightarrow 4^+$ and $5^- \rightarrow 4^+$ transitions have vanished. In panel c), where the condition is further lowered, practically only the $2^+ \rightarrow 0^+$ transition remains. A high condition on the TKEL enhances the intensities of the higher excited levels. This is demonstrated in panel d), where transitions that were not discernible in the first panel become visible. This is clearly appreciated in the intensity variation of the two components of the $2^+ \rightarrow 0^+$ transition, which is a short-lived transition ($0.35(2)\text{ps}$ [111]). Low TKEL values enhance the shifted component, while high TKEL values tend to increase the unshifted component due to the extra contribution from the feeders. More details on the determination and effects on the lifetime of a TKEL condition can be found in Ref. [107]

Other works involving lifetime measurements with the differential plunger using AGATA coupled to large acceptance magnetic spectrometers together with the use of the MNT mechanism to populate the excited states on the nuclei of interest, can be found in Refs. [112–120].

5.2 DSAM technique

The DSAM technique, illustrated in Fig. 8, allows for the investigation of lifetimes of excited states in the range of femtoseconds. The standard method requires a thin target deposited on a second thicker layer of a different material that acts as a stopper or as a degrader.

In the present case, in order to identify the MNT reaction products in the magnetic spectrometer, it is necessary to employ only thicknesses that will act as degraders. The information provided by the recoil is crucial for the identification of the nuclei in mass and atomic number but also for the kinematic reconstruction of the decaying nuclei, necessary for a Doppler correction on an event-by-event basis. In the energy range of a typical MNT reaction, states with

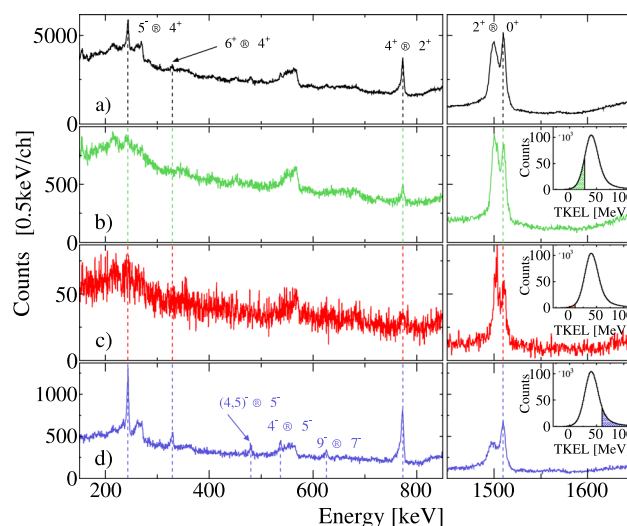


Fig. 7 Example of different TKEL conditions for ^{92}Mo using the shortest target-to-degrader distance. **a** Doppler-corrected spectrum without a TKEL condition. **b** Condition on the low part of the TKEL. **c** More restrictive condition on the low part of the TKEL. **d** Condition on the high part of the TKEL. Adapted from Ref. [110]

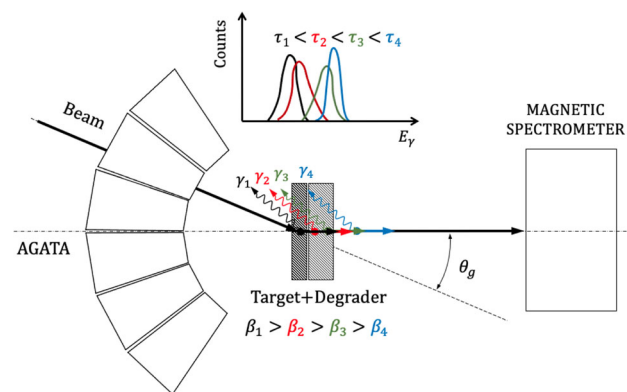


Fig. 8 Schematic view of the experimental set-up and description of the Doppler Shift Attenuation Method. The velocity used for the Doppler correction is the one measured by the magnetic spectrometer (β_4)

lifetimes below the femtosecond (τ_1 in Fig. 8) and picosecond (τ_4) range mainly decay within the target and after the degrader, respectively. These lifetimes are outside the range of sensitivity of the technique. Instead, γ rays emitted from the decay of states in the correct range, from tens to hundreds of femtoseconds (τ_2 and τ_3 , respectively, in Fig. 8) will be emitted by a decelerating ion within the degrader. The measured Doppler shift depends on the probability of emission at a specific velocity that, in turn, depends on the stopping power of the degrader and the amount of material crossed since the reaction point. The result is the presence in the γ -ray energy spectrum of a lineshape that is strongly correlated with the lifetime. The analysis and the inference of the lifetime rely on multiple Geant4 Monte Carlo simulations using

the AGATA Geant4 code [121] performed in a sensible range of lifetimes and energy of the γ -ray transition. The complete geometry of the apparatus and the experimental details, such as the intrinsic energy and position resolution, are optimised and included in the simulation, in order to reduce the sources of systematic error. The lifetime is then extracted by comparing the experimental response to the parametrised simulations by means of a least χ^2 or best likelihood [122] fitting. With respect to conventional γ -ray detector arrays, tracking arrays such as AGATA allow the continuous-angle analysis [123] and a better angular resolution. This is possible due to the AGATA position sensitivity resulting from a combination of contact segmentation, sampling of traces, Pulse Shape Analysis (PSA), and finally the application of tracking algorithms. The increased angular resolution allows one to access shorter lifetimes and also reduces the uncertainty of the lifetime measurement.

An example of this technique applied to MNT reaction is a recent experiment aimed at measuring the lifetimes of excited states around the $N = 20$ isotonic line. The experiment has been performed at LNL using PRISMA coupled to AGATA phase II, with 34 encapsulated detectors (12 ATC). A 230-MeV beam of ^{36}S impinged on a 1 mg/cm^2 -thick ^{208}Pb target, populating the neutron-rich region of the nuclear chart. The experiment was performed to further understand the transition probabilities of key states close to the so-called island of inversion, in particular in the ^{34}Si and ^{35}P nuclei, by means of DSAM. Although yrast states are the most favourably populated in MNT reactions, low-lying non-yrast states, suitable for DSAM measurements [124–127], were also observed. For this experiment, a 4 mg/cm^2 thick degrader of $^{\text{nat}}\text{Pd}$ was chosen to be sensitive to the expected lifetimes and to be able to detect the out-going ions in PRISMA. During the experiment, the region close to $N = 20$, $Z = 16$ has been successfully populated. From the preliminary analysis, it was observed that many transitions belonging to $^{36,37}\text{S}$, ^{35}P and ^{34}Si nuclei show the expected lineshape, indicating that the states they decayed from can be expected to have a lifetime in the range suitable for DSAM. An example can be seen in Fig. 9, where the $2_1^+ \rightarrow 0_{\text{g.s.}}^+$ transition of 3290 keV of ^{36}S is presented. A simulation performed assuming a lifetime of 0.12 ps [128] was performed and compared with the experimental data. The previously measured lifetime is supported by observed lineshape (Fig. 9) and will allow us to calibrate the technique for the unknown lifetimes to be determined in this experiment. However, the analysis is still preliminary and the simulation needs to be optimised in order to fit experimental data and reduce the sources of systematical errors.

For lifetimes studies of the excited states of nuclei in the same region with ranges going from the sub-picoseconds to several tens of picoseconds a slight modification can be done in the target to combine the DSAM method and the RDDS technique (see Sect. 5.1). For example, an experiment

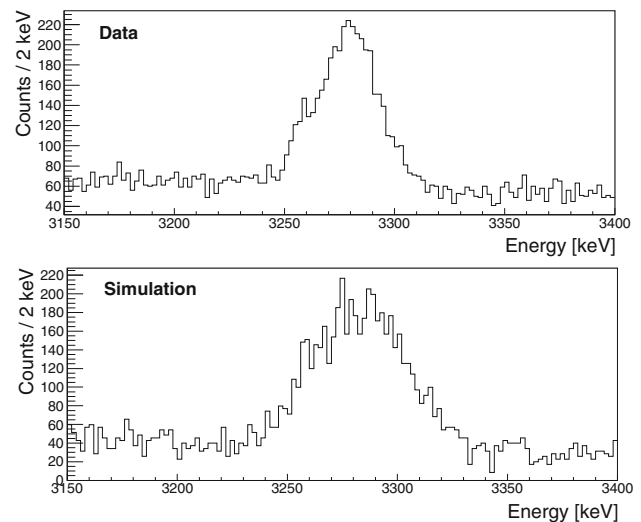


Fig. 9 Comparison between experimental (top) and simulated (bottom) lineshape of the $2_1^+ \rightarrow 0_{\text{g.s.}}^+$ of 3290 keV of ^{36}S . The simulation was performed using a lifetime of 0.12 ps, as measured in Ref. [128]

exploiting the combination of the two methods with AGATA coupled to PRISMA will be performed at LNL, during the phase II of AGATA, aiming to measure lifetimes around ^{48}Ca [129]. The nuclei of interest will be populated with the MNT reaction using a beam of ^{48}Ca at 300 MeV and a target of ^{238}U . The target of 1 mg/cm^2 thickness with a 3 mg/cm^2 Nb support layer (for DSAM) will be mounted together with the degrader of 4 mg/cm^2 of Nb (for RDDS) in a new compact plunger device [130]. Figure 10 illustrates the combination of the two techniques in ^{50}Ca with as GEANT4 simulation using the aforementioned Nb foils thicknesses for the support of the target and degrader. The $4^+ \rightarrow 2^+$ transition, 3488 keV, in ^{50}Ca was simulated varying the lifetime in the range of hundreds of femtoseconds. Due to the short lifetime simulated for the 4^+ , the state decays before the degrader and appears at a shifted energy after the Doppler correction using the velocity detected in PRISMA, but still is possible to appreciate the change in the line-shape for the DSAM technique (top panel in Fig. 10). The presence of the support layer in the target for DSAM (3 mg/cm^2 of Nb) does not influence the RDDS peak separation for the lifetime of 66.5 ps of the 2^+ state in ^{50}Ca [131] (bottom panel in Fig. 10).

5.3 DSAM technique with thick targets: lifetime measurements in light exotic nuclei

The use of the deep inelastic reactions opens the possibility to investigate excited states in neutron-rich nuclei in the sd -shell, such as B, C, N, O, and F nuclei, by employing, e.g. an ^{18}O beam on a heavy target (^{198}Pt or ^{238}U). For these nuclei the lifetimes of the excited states can be used as a testing ground for various theory approaches. For example, in the case of *ab initio* calculations a strong sensitivity of

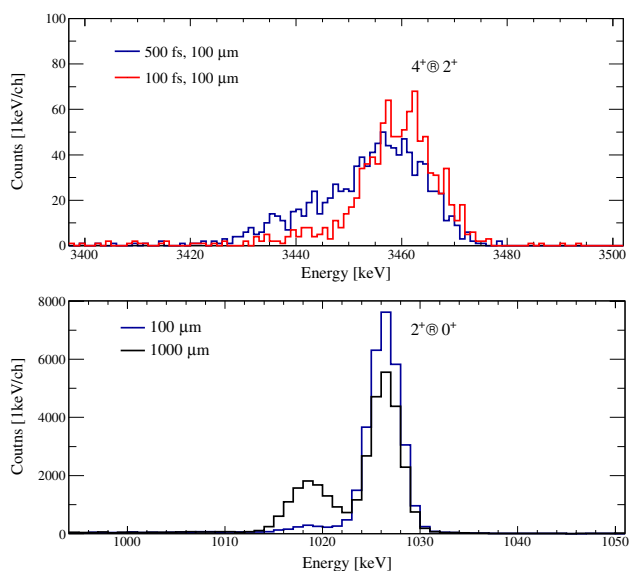


Fig. 10 Simulated Doppler corrected γ -ray spectra using the velocity from PRISMA (after the degrader) for ^{50}Ca showing the DSAM and RDDS techniques. Top, DSAM: line-shapes of the $4^+ \rightarrow 2^+$ transition varying the half-life. Bottom, RDDS: components before and after the degrader of the $2^+ \rightarrow 0^+$ transition for two distances using a half-life of 66.5 ps

the electromagnetic transition probabilities to the details of the nucleon–nucleon interactions, especially in connection with the role played by the three-body (NNN) forces, was predicted [132, 133].

Among the most interesting cases are ^{16}C and ^{18}C , for which *ab initio* calculations without and with the inclusion of the NNN term predict $B(E2)$ and $B(M1)$ of the second 2^+ states varying by a factor of 2 to 5. For example, for ^{16}C , the calculated lifetime of the second 2^+ state, with two-body (NN) forces only, is equal to 230 fs versus 80 fs with NN + NNN forces included. Similar calculations for ^{18}C provide a lifetime of ~ 2 ps versus ~ 1 ps considering NN or NN + NNN, respectively. Therefore, precise measurements of the lifetimes of the second 2^+ states in these systems, which require techniques able to extract lifetimes in the range of tens femtoseconds to few picoseconds, are needed.

A measurement has been performed at GANIL, using a set-up with AGATA coupled to VAMOS++ and PARIS [134], employing an ^{18}O beam at 7 MeV/u impinging on a thick ^{181}Ta target. A novel DSAM was developed which allows to assess tens-to-hundreds femtoseconds lifetimes of excited states in products of deep inelastic reactions [71, 135] using relatively thick target. With a thick target (several mg/cm^2), the velocity of the reaction product, measured with a magnetic spectrometer, does not correspond to the initial velocity in the exit channel, but it is the convolution of the complex structure of the product velocity distribution (caused by

large energy dissipation) and the slowing down process in the thick target material. It follows that standard DSAM cannot be directly employed. In such a case (thick target and deep inelastic processes), the procedure presented in Ref. [135] allows to reconstruct, via a Monte Carlo simulation, the reaction-product velocity distribution at the reaction instant, starting from the velocity measured by the magnetic spectrometer. The reconstructed velocity is then used to produce simulated Doppler-broadened γ -ray line shapes, to be compared with the experimental data. One has to stress that the quality of the results depends strongly on the Doppler-shift correction capabilities of the experimental set-up, namely the precision in the identification of the γ -ray interaction point in the HPGe crystal, and in the detection angle of the reaction products. With set-ups such as AGATA coupled to a magnetic spectrometer the angle between the fragment velocity at the de-excitation point and the γ -ray direction can be determined with an accuracy of about 1.5° , resulting in excellent sensitivity in γ -ray lineshape studies (see Fig. 22 and 23 of Ref. [135]).

The method of Ref. [135] was applied to extract the lifetime of the second 2^+ state in ^{20}O [71], and can be further employed to investigate the previously mentioned second 2^+ states in ^{16}C and ^{18}C , for example with AGATA + PRISMA at LNL, where the number of Ge crystals will provide much better conditions for reaching exotic species. Of great importance will be, in particular, the coverage of the angular range around 90° (between the reaction product velocity and γ ray emission directions), which will guarantee a precise γ -ray energy determination, not being Doppler affected. For this experiment, a thick target of ^{198}Pt ($\sim 10 \text{ mg}/\text{cm}^2$) could be used, and the magnetic spectrometer should be placed at the most forward possible angles, between 30° and 40° , to take advantage of the enhanced cross sections of deep-inelastic processes with respect to the grazing angle, as discussed in Sect. 2. The evaluation of the expected reaction cross section for ^{16}C and ^{18}C based on Deep Inelastic Transport (DIT) model calculations (see Fig. 3), gives $\sim 1 \text{ mb}/\text{sr}$ for ^{16}C , and $\sim 0.01 \text{ mb}/\text{sr}$ for ^{18}C ions, at $30 - 40^\circ$.

To extend the measurement to lifetime ranges up to a few ps, a further development of the DSAM method of Ciemala et al. [71, 135] could be considered. For this purpose, a thick degrader will be needed, at very close distance from the target. Figure 11 shows the expected lineshape of the 2217-keV $2_2^+ \rightarrow 2_1^+$ γ -ray of ^{16}C , as a function of the 2_2^+ state lifetime. These lineshapes are obtained from Geant4 simulations taking into account the reaction product velocities, the energy loss in the target and degrader, and the AGATA geometry. The simulation shows that a thick-target + thick-degrader configuration will result in a sensitivity for lifetime measurements from 80 fs to a few ps. It is worth noticing that, in such an experiment, a validation of the lifetime determination procedure, over the entire sensitivity range, could be obtained by

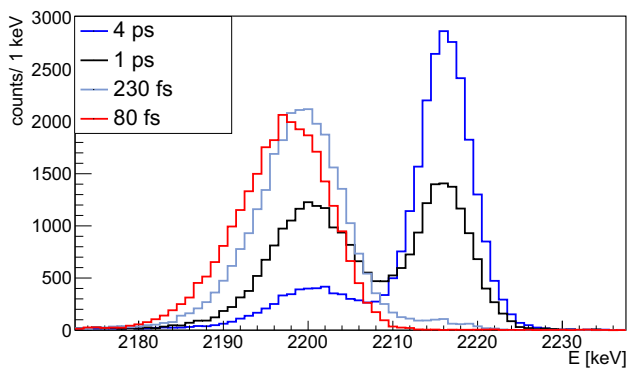


Fig. 11 Simulated Doppler corrected line-shapes of the 2217-keV γ ray, deexciting the second 2_2^+ state in ^{16}C , assuming lifetime values from 80 fs to 4 ps. The exotic ^{16}C nucleus is produced by a deep inelastic process induced by a ^{18}O beam (at 7 MeV/u) impinging on a ^{198}Pt target followed by a degrader (at 15 μm distance), both about 10 mg/cm² thick

using known level lifetimes in nearby nuclei, populated with similar deep inelastic reaction mechanisms. This is the case, for example, of the $1/2^+$ and $7/2^+$ states in the ^{19}O nucleus, with known lifetimes of 92 fs and 1.3 ps, respectively [131].

5.4 Geometrical DSAM technique

An additional method, to extend the range of lifetimes that can be measured with AGATA with Doppler techniques, is the so-called geometrical DSAM (geoDSAM) [123]. This technique is typically used to access lifetimes in the range from tens of picoseconds to few nanoseconds and it is suitable for reactions in which the velocity of the emitting fragments is between $0.3 < \beta < 0.8$ such as fragmentation. However, it can be used in reactions with lower velocities to measure longer lifetimes. This technique, illustrated in Fig. 12, is based on the Doppler shift due to the differences between the angle of emission and the angle used for the Doppler correction. States with short lifetimes decay in the proximity of the target and the angle θ_1 is similar to the one that is assumed for the Doppler correction, corresponding to the center of the target. States with longer lifetimes, instead, decay at a distance d from the target position. If the lifetime is sufficiently long, i.e. longer than tens of picoseconds, the difference between the real angle of emission θ_2 and the angle used for the Doppler correction generates a characteristic lineshape that depends on the β of the reaction product and on the lifetime of the excited states.

Lifetime measurements by means of geoDSAM have been performed in the past using the AGATA array to study the neutron-rich Mo isotopes via fragmentation reactions [136]. The measured values covered a range from a few to hundreds of picoseconds. The velocity involved in MNT reactions is typically around $\beta \approx 0.1$, hence the accessible lifetimes, using geoDSAM, are expected to be in a longer range. In the

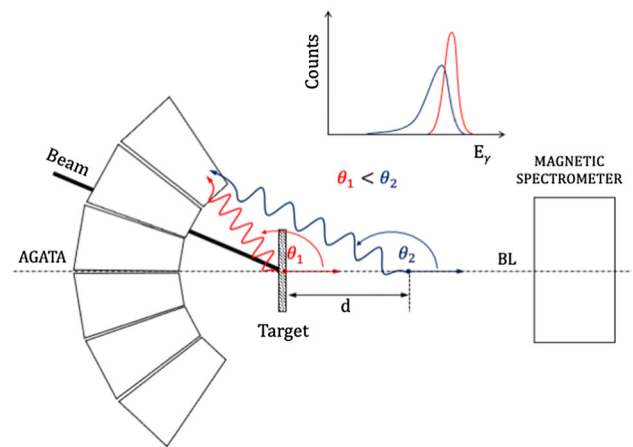


Fig. 12 Schematic view of the experimental set-up and description of the geometrical Doppler shift attenuation method

experiment described in Ref. [109], several states populated presented the characteristic lineshape of the geoDSAM. This indicated that the γ -ray emission was produced at a long distance after the target due to the lifetime being sufficiently long. As a consequence, the angle θ between the ion direction and the emitted γ ray is increased compared with the angle of γ -ray emission at the target position for a given first interaction position in AGATA. In the inelastic channel of the reaction described in Ref. [109], corresponding to ^{92}Mo , the 6^+ state, with a lifetime of 1.53(4) ns [131], de-excites to the 4^+ state with a γ ray of 329 keV. The experimental Doppler corrected spectrum for the $6^+ \rightarrow 4^+$ transition is shown with black circles in the top panel of Fig. 13. A full Monte-Carlo simulation with the corresponding AGATA configuration, reaction product velocity and with a half-life of 1.53 ns [131] is also presented in the Fig. 13 top panel, showing similar line-shape. The inelastic channel has been chosen to illustrate the technique due to the high statistics available, but this procedure is equivalent for the MNT channels. The bottom panel in the Fig. 13, shows the simulation of the geoDSAM effect that would be observed taking into account different half-lives for a γ -ray de-excitation around 300 keV. Even at this low energy the effect is visible and can be used to calculate lifetimes down to 500 ps.

5.5 Reversed plunger RDDS measurements

The isotope identification provided by PRISMA can be exploited to perform spectroscopic studies not only of the isotope directly detected by the spectrometer. In fact, in the case of a binary reaction, the kinematics of the undetected isotope can be reconstructed on the basis of the angle of entrance and the velocity measured by PRISMA. This, in turn, allows performing a Doppler correction on an event-by-event basis. This technique has been successfully exploited in the past

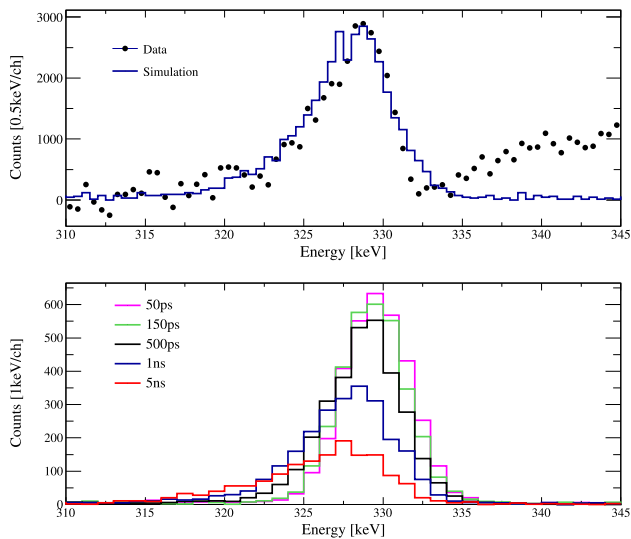


Fig. 13 Top: comparison between experimental (black circles) and simulated (blue line) lineshape for the $6^+ \rightarrow 4^+$ transition in ^{92}Mo . The simulation was performed using a lifetime of 1.53 ns [131]. Bottom: Simulated Doppler corrected line-shapes of a γ -ray de-excitation at 329 keV with variable half-life from 50 ps to 5 ns

and allowed the first measurement of γ rays linked to excited states of ^{196}Os and ^{200}Pt [137, 138].

A plunger device, in its standard configuration mentioned in Sect. 5.1 (i.e., a target followed by a degrader), is an excellent tool for measuring lifetimes of nuclear-excited states for a large number of nuclei with mass in the region where the PRISMA spectrometer has good atomic charge resolution ($\Delta Z/Z \simeq 1/60$). Presently, for nuclei with large Z and relatively small energy, unequivocal identification in the spectrometer becomes difficult. However, it is possible to extend the RDDS technique to heavier elements by using the plunger in the so-called “reversed configuration” identifying the lighter reaction product in the spectrometer and employing the binary-partner reconstruction. A schematic representation of this set-up configuration coupled to AGATA and the PRISMA spectrometer is shown in Fig. 14.

In this plunger configuration the degrader faces the beam, therefore, the beam passes through the degrader losing a part of its energy and then interacts with the target. The projectile-like fragment enters the spectrometer after crossing the target material with the shortest path, thus losing a minimal amount of energy that benefits its identification in the magnetic spectrometer. Meanwhile, the target-like fragment moves towards the degrader foil where it will be stopped. Consequently, one ends up in the same conditions as with the non-differential configuration of the plunger, with the ions of interest traveling between the target and the degrader at a given velocity. The γ rays will be emitted in flight or stopped, with a probability that depends on the lifetime of the state. If the lifetime of the state of interest is in the hundreds of picosec-

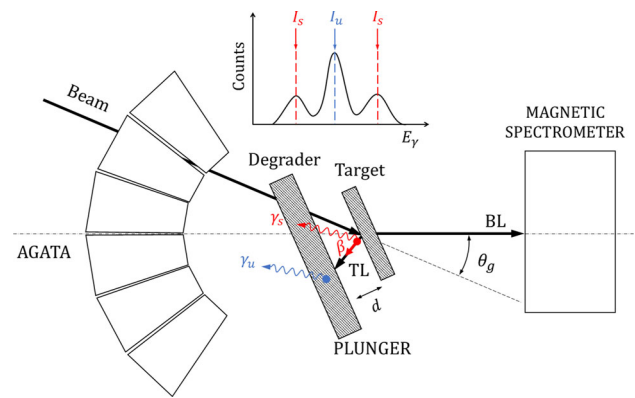


Fig. 14 Schematic representation of the plunger device in the reversed configuration coupled to AGATA and PRISMA

onds to nanoseconds range, the events will accumulate in two loci, when representing the γ -ray energy as a function of the angle between the emitting ion and the photon. Thanks to the position sensitivity of AGATA, the shifted and stopped components can be distributed in a continuous angular range. Performing measurements in several distances, the intensities of the shifted and the unshifted components of the peaks will allow the determination of the lifetime of the state of interest.

In the binary partner method, the detection of an isotope is not necessarily associated with a unique isotope as a binary partner, since the evaporation of several nucleons is a process that is more likely to occur after the transfer process. A condition on the total system excitation has proved to be successful, for the reduction of the contamination caused by the evaporation channels, in the spectroscopy measurement of ^{196}Os [137]. Additionally, gates in the TKEL also allow the substantial reduction of side feeding of higher-lying states in lifetime experiments.

In order to illustrate the technique, Geant4 simulations of the set-up were performed and are shown in Fig. 15. The energy of the simulated γ rays, corresponding to ^{92}Zr , populated via MNT reaction $^{93}\text{Nb}(^{34}\text{S}, ^{35}\text{Cl})^{92}\text{Zr}$, are plotted as a function of the angle between the reconstructed direction, as a binary partner, of the emitting ^{92}Zr fragments and the photon. The kinematics and thus the angle of emission of the target-like fragment, ^{92}Zr , depends on the angle of emission of its binary partner ion detected by PRISMA. It is possible to see in the figure that the in-flight and the stopped components are both present, and their separation is dependent on the relative angle, with an overlap that corresponds to 90° .

This technique has been successfully commissioned during the first campaign of AGATA phase II at LNL. The aim was to perform a measurement of the lifetime of the 4^+ state of ^{92}Zr . The state of interest was populated via MNT reaction. A beam of ^{34}S impinged in a ^{93}Nb target. Projectile-like particles, ^{35}Cl , were detected by PRISMA placed at the graz-

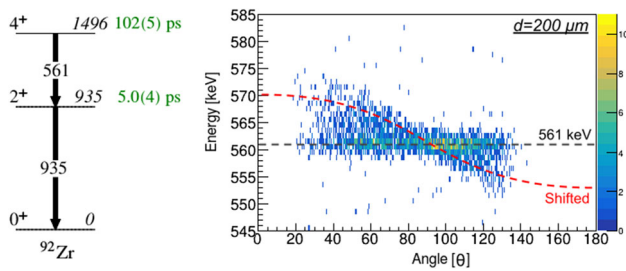


Fig. 15 (Left) Partial level scheme of ^{92}Zr . (Right) Geant4 simulations for reversed plunger measurement. Gamma rays of ^{92}Zr , populated via MNT reaction $^{93}\text{Nb}(^{34}\text{S},^{35}\text{Cl})^{92}\text{Zr}$, are plotted as a function of the relative angle between the γ -ray and the ion. Simulations were performed for a plunger distance of $200\ \mu\text{m}$

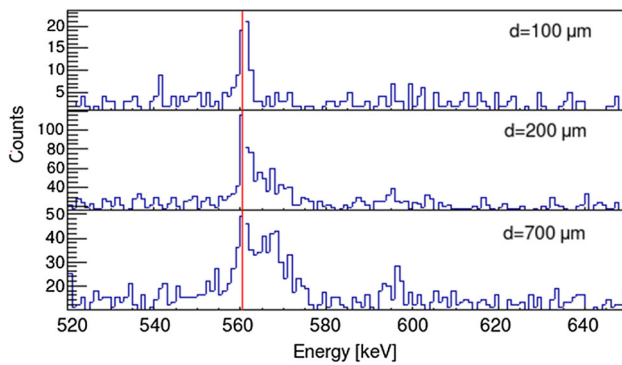


Fig. 16 The experimental γ -ray spectrum of ^{92}Zr measured from AGATA (from 0 to 60 degrees ring) in coincidence with PRISMA for different distances between the target and the degrader. The stopped component of the $4^+ \rightarrow 2^+$ 561-keV transition of ^{92}Zr is indicated with the red line

ing angle at 40° , meanwhile, target-like particles stopped in a $3\ \text{mg}/\text{cm}^2$ -thick Ta stopper foil. Gamma rays are measured with AGATA composed of 32 encapsulated detectors. The experimental γ -ray spectrum of ^{92}Zr measured from AGATA array (from 0 to 60 degrees ring), in coincidence with PRISMA for different distances between the target and the degrader is shown in Fig. 16. The stopped component, the 561-keV peak ($4^+ \rightarrow 2^+$ transition of ^{92}Zr) is indicated with a red line. As can be seen, the intensity of the Doppler-shifted peak rises as increasing the distance. The analysis of the data from this experiment is still in progress but the preliminary spectrum, shown in the latter figure, demonstrates that the two γ -ray components in the spectrum emerging from the decay of the nucleus in flight or stopped can be separated by using the plunger in such configuration. The use of this technique creates new possibilities for lifetime measurements of nuclear-excited states in heavy ions produced in MNT reactions that can not be well identified in the magnetic spectrometer, allowing one to reach nuclei in regions of the nuclear chart yet to be explored.

6 Summary outlook and conclusions

This work discusses the capabilities of set-ups including AGATA, coupled with large acceptance magnetic spectrometers as PRISMA and VAMOS++, for the experimental research in nuclear structure employing multi-nucleon transfer reactions in quasi-elastic and deep-inelastic regimes. Particularly relevant is the possibility to perform lifetime measurements with Doppler techniques, in neutron-deficient and well as neutron-rich nuclei, limiting the contribution of the side-feeding with conditions in the TKEL measured by the spectrometers. The mechanism of the MNT reactions and the expectations of reaching even further away from stability using unstable beams provided by re-accelerated ISOL facilities is a relevant aspect to be considered in future campaigns of AGATA coupled with PRISMA and VAMOS++. AGATA opens new possibilities of precision measurements in nuclear structure providing a wealth of experimental information.

Recently, there is an increasing interest on the MNT mechanism suggesting its use to approach the ^{100}Sn region [139], to study the heavy neutron-rich nuclei associated with the nucleosynthesis [140] as well as to populate very heavy and superheavy nuclei [141, 142]. With MNT one could take advantage of the reconstruction of the reaction Q value and the typical low recoil velocity ($v/c \sim 10\%$) to perform high-resolution γ spectroscopy and lifetime measurements below the low-lying isomers, that are present in many nuclei in these regions.

While these ideas are mostly based on theoretical calculations that require experimental confirmation and represent experimental challenges, nevertheless, they suggest extension of conventional experimental activity in regions that might become accessible with the increasing efficiency of our state-of-the-art instrumentation together with high-intensity stable and radioactive ion beams.

Acknowledgements The authors acknowledge the scientific and instrumental contribution of the AGATA, PRISMA and VAMOS++ collaborations to this work. The experimental activity, discussed in this article, has been performed at INFN - Laboratori Nazionali di Legnaro, Italy and Grand Accélérateur National d'Ions Lourds, France. The authors are indebted to the accelerator, technical and scientific staff of these laboratories for their contribution to the success of the experimental activities. This work was partially supported by MCIN/AEI/10.13039/501100011033, Spain with Grant PID2020-118265GB-C42, by Generalitat Valenciana, Spain with grants PROMETEO/2019/005, CIBEST/2021/210 and CIAPOS/2021/114 and by the EU FEDER funds. Work partially supported by the Croatian Science Foundation project No. IP-2018-01-1257 and by the Center of Excellence for Advanced Materials and Sensing Devices, Grant No. KK.01.1.1.01.0001. This research was also supported by the U.S. Department of Energy, Office of Science, Office of Nuclear Physics, under contract number DE-AC02-06CH11357.

Funding Information Open Access funding provided thanks to the CRUE-CSIC agreement with Springer Nature.

Data Availability Statement This manuscript has no associated data or the data will not be deposited. [Authors' comment: The data generated in this study are contained in the publication.]

Open Access This article is licensed under a Creative Commons Attribution 4.0 International License, which permits use, sharing, adaptation, distribution and reproduction in any medium or format, as long as you give appropriate credit to the original author(s) and the source, provide a link to the Creative Commons licence, and indicate if changes were made. The images or other third party material in this article are included in the article's Creative Commons licence, unless indicated otherwise in a credit line to the material. If material is not included in the article's Creative Commons licence and your intended use is not permitted by statutory regulation or exceeds the permitted use, you will need to obtain permission directly from the copyright holder. To view a copy of this licence, visit <http://creativecommons.org/licenses/by/4.0/>.

References

1. A.G. Artukh et al., Nucl. Phys. A **160**, 511 (1971)
2. R.M. Diamond et al., Phys. Rev. Lett. **20**, 802 (1968)
3. K. Van Bibber et al., Phys. Rev. Lett. **38**, 334 (1977)
4. H. Puchta et al., Phys. Rev. Lett. **43**, 623 (1979)
5. W. Trautmann et al., Nucl. Phys. A **422**, 418 (1984)
6. R. Kirchner et al., Nucl. Phys. A **378**, 549 (1982)
7. E. Runte et al., Nucl. Phys. A **399**, 163 (1983)
8. U. Bosch et al., Phys. Lett. B **164**, 22 (1985)
9. R. Broda et al., Phys. Lett. B **251**, 245 (1990)
10. R. Broda et al., Phys. Rev. Lett. **74**, 868 (1995)
11. R.H. Mayer et al., Z. Phys. A **342**, 247 (1992)
12. M. Rejmund et al., Z. Phys. A **359**, 243 (1997)
13. J.F.C. Cocks et al., Phys. Rev. Lett. **78**, 2920 (1997)
14. H. Savajols, and Vamos Collaboration. Nucl. Phys. A **654**, 1027c (1999)
15. M. Rejmund et al., Nuclear Instruments and Methods in Physics Research Section A: Accelerators, Spectrometers, Detectors and Associated Equipment **646**, 184–191 (2011)
16. Y. Son et al., EMIS 2022 conference proceeding, submitted to Nuclear Instruments and Methods in Physics Research Section B (2023)
17. A.M. Stefanini et al., Nucl. Phys. A **701**, 217 (2002)
18. S. Szilner et al., Phys. Rev. C **76**, 024604 (2007)
19. J. Simpson et al., Acta Physica Hungarica, Series A: Heavy Ion. Physics **11**, 159 (2000)
20. A. Gadea et al., Eur. Phys. J. A **20**, 193 (2003)
21. A. Gadea et al., Nucl. Instr. Methods Phys. Res. A **654**, 88 (2011)
22. E. Clément et al., Nucl. Instr. Methods Phys. Res. Sect. A, **855**, 1 (2017)
23. J. J. Valiente-Dobón et al., Nucl. Instr. Methods Phys. Res. A **168040** (2023)
24. J.J. Valiente-Dobón et al., Phys. Rev. Lett. **102**, 242502 (2009)
25. L. Corradi, G. Pollarolo, S. Szilner, J. of Phys. G **36**, 113101 (2009)
26. T. Mijatović, Front. Phys. **10**, 965198 (2022)
27. A. Gadea, Eur. Phys. J. A **25**, 421 (2005)
28. A. Bracco, G. Duchêne, Zs. Podolyak and P. Reiter, Progress in Particle and Nuclear Physics **121**, 103887 (2021)
29. S. Lunardi et al., Phys. Rev. C **76**, 034303 (2007)
30. D. Montanari et al., Phys. Lett. B **697**, 288 (2011)
31. S. Szilner et al., Phys. Rev. C **84**, 014325 (2011)
32. M. Varga Pajtler et al., Nucl. Phys. A **941**, 273 (2015)
33. D.M. Brink, Phys. Lett. B **40**, 37 (1972)
34. B. Fornal et al., Phys. Rev. C **77**, 014304 (2008)
35. J.J. Valiente-Dobón et al., Phys. Rev. C **78**, 024302 (2008)
36. X. Liang et al., Phys. Rev. C **74**, 014311 (2006)
37. R. Chapman et al., Phys. Rev. C **92**, 044308 (2015)
38. C.H. Dasso, G. Pollarolo, A. Winther, Phys. Rev. Lett. **73**, 1907 (1994)
39. V. Zagrebaev, W. Greiner, Phys. Rev. Lett. **101**, 122701 (2008)
40. K. Sekizawa, K. Yabana, Phys. Rev. C **88**, 014614 (2013)
41. K. Sekizawa, K. Yabana, Phys. Rev. C **93**, 054616 (2016)
42. K. Sekizawa, Phys. Rev. C **96**, 014615 (2017)
43. K. Sekizawa, Phys. Rev. C **96**, 041601 (2017)
44. C. Simenel, Phys. Rev. Lett. **105**, 192701 (2010)
45. C. Simenel, K. Godbey, A.S. Umar, Phys. Rev. Lett. **124**, 212504 (2020)
46. C. Simenel, A.S. Umar, Prog. Part. Nucl. Phys. **103**, 19 (2018)
47. Y.X. Watanabe et al., Phys. Rev. Lett. **115**, 172503 (2015)
48. A. Vogt et al., Phys. Rev. C **92**, 024619 (2015)
49. P.R. John et al., Phys. Rev. C **95**, 064321 (2017)
50. T. Mijatović et al., Phys. Rev. C **94**, 064616 (2016)
51. F. Galtarossa et al., Phys. Rev. C **97**, 054606 (2018)
52. P. Čolović et al., Phys. Rev. C **102**, 054609 (2020)
53. A. Winther, Nucl. Phys. A **572**, 191 (1994). A. Winther, Nucl. Phys. A **594**, 203 (1995)
54. S. Szilner et al., Phys. Rev. C **71**, 044610 (2005)
55. L. Corradi et al., Phys. Rev. C **66**, 024606 (2002)
56. K. Gorički, M. Sc, *thesis* (University of Zagreb, Faculty of Science, 2020). ((unpublished))
57. J. Eberth et al., Prog. Part. Nucl. Phys. **46**, 389 (2001)
58. D. Montanari et al., Phys. Rev. Lett. **113**, 052501 (2014)
59. D. Montanari et al., Phys. Rev. C **93**, 054623 (2016)
60. L. Corradi et al., Phys. Lett. B **834**, 137477 (2022)
61. R. Broda, J. Phys. G: Nucl. Part. Phys. **32**, R151 (2006)
62. A. Gobbi, W. Norenberg, Heavy Ion Collisions vol 2, ed. R. Bock, Amsterdam: North-Holland, 1980
63. L. Tassan-Got, C. Stéphan, Nucl. Phys. A **524**, 121 (1991)
64. V.I. Zagrebaev, W. Greiner, J. Phys. G **34**, 1 (2007)
65. R. Broda et al., Phys. Rev. C **98**, 024324 (2018)
66. K.E. Rehm, A.M. van den Berg, J.J. Kolata, D.G. Kovar, W. Kutschera, G. Rosner, G.S.F. Stephans, J.L. Yntema, Phys. Rev. C **37**, 2629 (1988)
67. J. Diklić et al., Phys. Rev. C **107**, 014619 (2023)
68. G.J. Balster et al., Nucl. Phys. A **468**, 93 (1987)
69. G.J. Balster et al., Nucl. Phys. A **468**, 131 (1987)
70. S. Bottoni et al., Phys. Rev. **85**, 064621 (2012)
71. M. Ciemała et al., Phys. Rev. C **101**, 021303(R) (2020)
72. S. Ziliani et al., Phys. Rev. C **104**, L041301 (2021)
73. V.I. Zagrebaev, B. Fornal, S. Leoni, and Walter Greiner. Phys. Rev. C **89**, 054608 (2014)
74. I. Stefan et al., Phys. Lett. B **779**, 456 (2018)
75. R. Anne et al., Nucl. Instrum. Methods A **257**, 215 (1987)
76. A.V. Karpov, V.V. Saiko, Phys. Rev. C **96**, 024618 (2017)
77. V.I. Zagrebaev, Y. Aritomo, M.G. Itkis, Yu.Ts. Oganessian, M. Ohta, Phys. Rev. C **65**, 014607 (2001)
78. R.J. Charity, Phys. Rev. C **82**, 014610 (2010)
79. G.A. Souliotis et al., Phys. Lett. B **543**, 163 (2002)
80. G.A. Souliotis et al., Nucl. Instrum. Methods A **1031**, 166588 (2022)
81. R.E. Tribble, R.H. Burch, C.A. Gagliardi, Nucl. Instrum. Methods A **285**, 441 (1989)
82. A. Cunsolo et al., Nucl. Instr. and Meth. A **481**, 48 (2002)
83. A. Cunsolo et al., Nucl. Instr. and Meth. A **484**, 56 (2002)
84. L. Corradi et al., Phys. Rev. C **59**, 261 (1999)
85. L. Corradi et al., Nucl. Instrum. Methods B **317**, 743 (2013)
86. S. Akkoyun et al., Nucl. Instr. Methods Phys. Res. Sect. A **668**, 26 (2012)
87. A. Andrighetto et al., J. Phys: Conf. Ser. **966**, 012028 (2018)
88. M. Lewitowicz, J. Phys: Conf. Ser. **312**, 052014 (2011)

89. D. Ralet et al., Phys. Lett. B **797**, 134797 (2019)
90. B. Birkenbach et al., Phys. Rev. C **92**, 044319 (2015)
91. E. Fioretto et al., Nucl. Inst. Methods Phys. Res. A **899**, 73 (2018)
92. F. Rybicki, T. Tamura, G.R. Satchler, Nucl. Phys. A **146**, 659 (1970)
93. T. Døssing, Nucl. Phys. A **357**, 488 (1981)
94. G.R. Young et al., Phys. Rev. C **25**, 1304 (1982)
95. P. Aguer et al., Phys. Rev. Lett. **43**, 1778 (1979)
96. D. V.Harrach et al., Phys. Rev. Lett. **42**, 1728 (1979)
97. D. Bucurescu et al., Phys. Rev. C **76**, 064301 (2007)
98. D. Bazzacco, in: Proc. Int. Conf. on Nuclear Structure at High Angular Momentum, Ottawa, vol. 2, AECL 10613, 1992, p. 316
99. H.J. Rose, D.M. Brink, Rev. Mod. Phys. **39**, 306 (1967)
100. E. Der Mateosian, A.W. Sunyar, At. Data Nucl. Data Tables **13**, 391 (1974)
101. D. Montanari, S. Leoni et al., Phys. Rev. C **85**, 044301 (2012)
102. E. Sahin et al., Nucl. Phys. A **893**, 1 (2012)
103. F.C.L. Crespi et al., Phys. Rev. Lett. **113**, 012501 (2014)
104. F.C.L. Crespi et al., AGATA: Performance of gamma-ray tracking and associated algorithms in this issue
105. A. Dewald, O. Möller, P. Petkov, Prog. Part. Nucl. Phys. **67**, 786 (2012)
106. A. Schwarzschild, E. Warburton, Annu. Rev. Nucl. Sci. **18**, 265 (1968)
107. M. Siciliano, J. J. Valiente-Dobón, A. Goasduff, EPJ: Web Conf. **223**, 01060 (2019)
108. S. Szilner et al., Phys. Rev. C **76**, 024604 (2007)
109. R.M. Pérez-Vidal et al., Phys. Rev. Lett. **129**, 112501 (2022)
110. R. M. Pérez-Vidal, Ph.D thesis, Universidad de Valencia, 2019
111. P.H. Stelson et al., Bull. Am. Phys. Soc. **9**, 484 (1964)
112. M. Siciliano et al., Phys. Lett. B **806**, 135474 (2020)
113. M. Siciliano et al., Phys. Rev. C **104**, 034320 (2021)
114. A. Goldkuhle et al., Phys. Rev. C **100**, 054317 (2019)
115. A. Goldkuhle et al., Phys. Rev. C **102**, 054334 (2020)
116. D. Ralet et al., Phys. Lett. B **797**, 134797 (2019)
117. V. Modamio et al., Phys. Rev. C **88**, 044326 (2013)
118. M. Doncel et al., Eur. Phys. J. A **53**, 211 (2017)
119. E. Sahin et al., Phys. Rev. C **91**, 034302 (2015). Phys. Rev. C **95**, 024312 (2017)
120. M. Klintejord et al., Phys. Rev. C **95**, 024312 (2017)
121. E. Farnea et al., Nucl. Instr. and Meth. A **621**, 331 (2010)
122. M. Tanabashi et al., Review of Particle Physics. Phys. Rev. D **98**, 030001 (2018)
123. C. Stahl, J. Leske, M. Lettmann, N. Pietralla, Comp. Phys. Comm. **214**, 174 (2017)
124. L. Grucutt et al., Phys. Rev. C **100**, 064308 (2019)
125. L. Grocutt et al., Phys. Rev. C **106**, 024314 (2022)
126. R.W. Ibbotson et al., Phys. Rev. Lett. **80**, 2081 (1998)
127. M. Wiedeking et al., Phys. Rev. C **78**, 037302 (2008)
128. K.-H. Speidel et al., Phys. Lett. B **659**, 101 (2008)
129. C. Fransen, A. Gottardo, D. Mengoni et al., Proposal accepted 2022: Lifetime measurements around ^{48}Ca AGATA-PRISMA-PLUNGER
130. M. Beckers et al., Nucl. Instr. Meth. A **1042**(5), 167418 (2022)
131. National Nuclear Data Center, <https://www.nndc.bnl.gov/ENSDFandXUNDL>
132. C. Forssen et al., J. Phys. G: Nucl. Part. Phys. **40**, 055105 (2013)
133. P. Voss et al., Phys. Rev. C **86**, 011303(R) (2012)
134. A. Maj, F. Azaiez, D. Jenkins, Acta Phys. Pol., B **40**, 565 (2009)
135. M. Ciemała et al., Eur. Phys. J. A **57**, 156 (2021)
136. D. Ralet et al., Phys. Rev. C **95**, 034320 (2017)
137. P.R. John et al., Phys. Rev. C **90**, 021301 (2014)
138. P.R. John et al., Phys. Rev. C **95**, 064321 (2017)
139. Z. Wu, L. Guo, Z. Liu, G. Peng, Phys. Lett. B **825**, 136886 (2022)
140. S. Heinz, H.M. Devaraja, Eur. Phys. J. A **58**, 114 (2022)
141. A. Karpov, V. Saiko, Phys. Part. Nucl. Lett. **16**, 667 (2019)
142. X.J. Bao, Phys. Rev. C **104**, 034604 (2021)